Journal of Power Sources 285 (2015) 469–477

Contents lists available at ScienceDirect

Journal of Power Sources

journal homepage: www.elsevier.com/locate/jpowsour

Mesoporous carbon spheres with controlled porosity for high-performance lithium–sulfur batteries

Dexian Wang [a], Aiping Fu [a], Hongliang Li [a, *], Yiqian Wang [b], Peizhi Guo [a], Jingquan Liu [a], Xiu Song Zhao [a, c]

[a] Collaborative Innovation Center for Marine Biomass Fibers, Materials and Textiles of Shandong Province, Laboratory of New Fiber Materials and Modern Textile, Growing Base for State Key Laboratory, College of Chemical Science and Engineering, Qingdao University, No. 308 Ningxia Road, Qingdao 266071, China

[b] College of Physics, Qingdao University, No. 308 Ningxia Road, Qingdao, 266071, China

[c] School of Chemical Engineering, The University of Queensland, St Lucia, Brisbane, QLD 4072, Australia

HIGHLIGHTS

- Spray drying was applied to the preparation of porous carbon microspheres.
- The porous carbon microspheres possess hierarchical pores and controlled porosity.
- The porous carbon had been used as support for sulfur with content up to 80 wt%.
- A high pressure process was applied to the impregnation of sulfur into the pores.
- The obtained Li–S batteries showed excellent electrochemical performance.

GRAPHICAL ABSTRACT

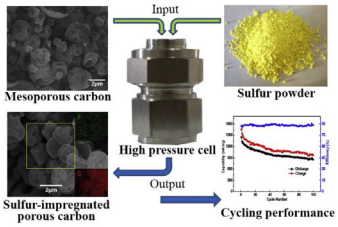

ARTICLE INFO

Article history:
Received 21 December 2014
Received in revised form
18 March 2015
Accepted 22 March 2015
Available online 23 March 2015

Keywords:
Lithium–sulfur battery
Porous carbon spheres
Hierarchical pores
Spray drying
Sodium alginate

ABSTRACT

Mesoporous carbon (MC) spheres with hierarchical pores, controlled pore volume and high specific surface areas have been prepared by a mass-producible spray drying assisted template method using sodium alginate as carbon precursor and commercial colloidal silica particles as hard template. The resulting MC spheres, possessing hierarchical pores in the range of 3–30 nm, are employed as conductive matrices for the preparation of cathode materials for lithium–sulfur batteries. A high pressure induced one-step impregnation of elemental sulfur into the pore of the MC spheres has been exploited. The electrochemical performances of sulfur-impregnated MC spheres (S-MC) derived from MC spheres with different pore volume and specific surface area but with the same sulfur loading ratio of 60 wt% (S-MC-X-60) have been investigated in details. The S-MC-4-60 composite cathode material displayed a high initial discharge capacity of 1388 $mAhg^{-1}$ and a good cycling stability of 857 $mAhg^{-1}$ after 100 cycles at 0.2C, and shows also excellent rate capability of 864 $mAhg^{-1}$ at 2C. More importantly, the sulfur loading content in MC-4 spheres can reach as high as 80%, and it still can deliver a capacity of 569 $mAhg^{-1}$ after 100 cycles at 0.2C.

© 2015 Elsevier B.V. All rights reserved.

* Corresponding author.
E-mail address: lhl@qdu.edu.cn (H. Li).

http://dx.doi.org/10.1016/j.jpowsour.2015.03.135
0378-7753/© 2015 Elsevier B.V. All rights reserved.

1. Introduction

Lithium ion battery (LIB) is one of the most popular power sources for portable electric devices and energy storage systems due to its high energy density, high operating voltage and low self-discharge. However, the limited energy capacity and low power density at the cell level do not meet the requirements for electric vehicles [1,2]. Lithium–sulfur (Li–S) batteries have attracted increasing interest during the last decade due to their high theoretical capacity of 1672 $mAhg^{-1}$, which is nearly five times higher than that of the existing transition metal oxide and phosphate materials [3,4]. In addition, elemental sulfur is readily available and nontoxic, and has many advantages that should allow to produce cheap and safe high energy batteries [5]. However, in spite of these advantages, there are still a number of issues associated with the commercialization of Li–S batteries, such as the electrical insulating nature of sulfur and the high solubility of lithium polysulfides, especially the intermediate products formed during the discharge process in traditional organic electrolyte, which results in a shuttle effect and leads to poor cycle life of the cells [6–8]. Therefore, enhancing the cycling performance and improving sulfur utilization are two important challenges with respect to the realization of high energy Li–S batteries.

In response to these challenges, strategies have been demonstrated for solving these problems, such as surface coating [9–11], conductive substrates [12–20], multifunctional binders and novel electrolytes with inorganic additives [21–23]. Among the above strategies, carbon-based materials with controlled morphology and structure, particularly those derived from cheap sustainable sources constitute a rational solution for the preparation of practical carbon–sulfur composite electrodes [17]. In comparison with other carbon materials such as graphene [14] and carbon nanotubes [15], porous carbon materials can strongly absorb polysulfides and buffer the volume expansion of sulfur due to the presence of pores [12,13,18], leading to improved cycle life and columbic efficiency. Moreover, porous carbon materials can be prepared in a relatively simple, effective and scalable way. The main synthetic methods of mesoporous carbon could be summarized as follows [24]: (a) carbonization of carbon precursors composed of one thermosetting component and one thermally unstable component [19], (b) catalyst-assisted activation of carbon precursors with metal (oxides) or organometallic compounds, (c) carbonization of aerogels or cryogels, (d) replication synthesis with pre-synthesized hard templates through impregnation, carbonization and template removal [20], and (e) self-assembly using soft templates through co-condensation and carbonization. In most cases, researchers mainly concentrated on method (a) and (d). So far, many studies have performed on porous carbon materials with different pore sizes including micropore, mesopore and macropore. For example, It has been demonstrated that the electrochemical reaction process of the sulfur cathode can be constrained inside the micropores of porous carbon sphere with a narrow micropore size distribution of about 0.7 nm, resulting in good reversibility and excellent high rate discharge capability [25]. However, the sulfur loading ratio or loading method may be limited due to the low mesopore volume. Although porous carbon material with a relatively large amount of macropores posses a high discharge capacity, the presence of macropores is usually responsible for rapid loss of capacity with cycling [26]. Therefore, the unique mesopore is an ideal volume for achieving both high sulfur loading and excellent electrochemical performance. However, the preparation processes, especially those for porous carbon in spherical morphology with mesosized pores are always complicated and the precursors are expensive or poisonous, which then hinder the practical applications of mesoporous carbon spheres in large. In addition, even though several ways, such as thermal treatment [19], precipitation method [27] and CS_2 solution adsorption [20], to loading sulfur into the pore of porous carbon matrices have been developed, but most of the procedures are tedious or use poisonous solvent, limiting also the practical application of sulfur-impregnated porous carbon spheres in Li–S batteries.

In this work, we reported on a flexible and mass-producible approach to the fabrication of sulfur-impregnated porous carbon composite cathode materials for high performance Li–S batteries. As a well-developed industrial method, spray drying method has been extensively utilized in fabrication of powders or particles of a variety of materials, especially those are temperature sensitive, for example food additives, flower or plant extracting ingredients. Herein, mesoporous carbon (MC) spheres with mesosized hierarchical pores in the range of 3–30 nm, controlled pore volume and relatively high specific surface area were prepared through a spray drying assisted template method by combing a separated carbonization process. Sodium alginate (SA) was chosen as the precursor for carbon and nanosized silica particles (in colloid) were used as hard template to direct the pores inside the carbon spheres. In comparison with the documented preparation methods or processes for porous carbon, the spray drying assisted template method is relatively simple, flexible and easily scalable, which is also different from the reported spray paralysis method although both of them concern a spray process. The resulted MC spheres were then exploited as the matrix for fabricating sulfur-impregnated mesoporous carbon composite spheres (S-MC). An autogenetic pressure technique at high temperature based on a swagelok structured stainless autoclave was exploited for loading sulfur into the pores of the MC spheres. By using this autogenetic pressure technique, sulfur-impregnated mesoporous carbon spheres (S-MC) with controlled sulfur loading content were obtained efficiently. No extra heating process to remove the excess sulfur was required. The sulfur-impregnated mesoporous carbon spheres were then used as cathode materials for Li–S batteries. Electrochemical measurements demonstrated that the S-MC composite materials could improve both cycling performance and rate capability of the sulfur cathode, while in the meantime retard the polysulfide induced shuttle phenomenon.

2. Experimental section

2.1. Materials

Sodium alginate (SA), acetic acid, hydrofluoric acid (30 wt %), ethanol and sulfur (Sinopharm Chemical Reagent Co., Ltd) were of AR grade and used without further purification. Colloidal silica (GRACE LUDOX, AS-30, 30%, ~12 nm, U.S.A), kindly provided by Cheng Song International Trading (Shanghai) Co., Ltd, was used as received without further treatment.

2.2. Preparation of MC spheres

The MC spheres were prepared by a spray drying assisted template method using SA as a carbon precursor and nanosized silica particles as hard template through a laboratory-scale SP-1500 spray dryer (Shanghai SunYi Tech Co., Ltd.). In a typical preparation, 2 g of SA was dissolved in 350 mL of 5 wt % acetic acid aqueous solution, and then an amount of designed silica colloids was added into the SA aqueous solution. The mixture was then stirred for 2 h to obtain a stable and clear suspension. After that, the solution was sprayed into the chamber of the spray dryer at 180 °C using hot air as carrier gas, and dried silica/SA composite microspheres were simultaneously collected by a connected cyclone separator. Then, the obtained silica/SA composite spheres were firstly cured at

400 °C for 2 h and then carbonized at 900 °C for 5 h under a high-purity nitrogen atmosphere to obtain the silica/carbon composite spheres. After the autoclave was cooled down to room temperature naturally, silica/carbon composite spheres were collected. Then 20 wt% HF aqueous solution was used to etch the silica particles inside the resulting silica/carbon composite spheres for 24 h at room temperature. After washing thrice with distilled water and ethanol, respectively, the products were dried at 120 °C for 12 h in air, yielding 60% black MC spheres by weight based on the carbon content in the SA. MC samples derived from silica/SA composite spheres made with different volumes of silica colloid of 2, 3, 4 and 5 mL were designated as MC-X spheres (where X = 2, 3, 4 and 5, respectively), and their yields decreased slightly with the increase of the silica/SA ratio.

2.3. Preparation of S-MC composite spheres

The S-MC composite spheres with different sulfur loadings, for example 60 and 80 wt% were prepared by firstly grinding sulfur with the above obtained MC-X spheres, and then the homogenous mixture was transferred into a stainless autoclave and sealed with a swagelok structured cover. The autoclave was treated at 155 °C for 5 h firstly, and then the temperature was increased to 300 °C and kept for 5 h to guarantee that the melted sulfur was infiltrated into the pores of MC spheres completely under the autogenetic pressure. The resultant S-MC composite spheres derived from MC-X (X = 2, 3, 4 and 5) spheres with different sulfur loading contents, e.g. 60 and 80 wt%, were denoted as S-MC-X-W composite spheres (where W = 60 and 80, respectively). The loading content of sulfur was defined based on the total mass of the composite spheres. A proposed formation mechanism of the S-MC composite spheres is illustrated in Scheme 1.

2.4. Characterization

The crystallographic information and composition of the products were investigated using a Bruker D8 Advance X-ray diffractometer (XRD, Cu-Kα radiation λ = 0.15418 nm). Raman spectra were collected using a Horiba LabRAM HR Raman spectrometer (HORIBA Jobin Yvon Ltd.). The specific surface areas were estimated with the Brunauer–Emmett–Teller (BET) method with N_2 adsorption data in the relative pressure range of P/P_0 = 0.05–0.35. The pore size distributions were calculated using the Barrett–Joyner–Halenda (BJH) model applied to the desorption branch of the N_2 isotherms obtained with a TriStar 3000 surface area and pore analyzer (Micromeritics). The morphology and structure of the samples were examined by a JEOL JSM-6390LV scanning electron microscope (SEM) and a JEOL JEM-2010F transmission electron microscope (TEM).

2.5. Electrochemical measurement

The working electrodes were prepared by a slurry coating procedure. The slurry consisting of 80 wt% of S-MC-X-W composite spheres, 10 wt% carbon conductive agents (acetylene black) and 10 wt% polyvinylidene fluoride (PVDF) was coated on an aluminum foil. After drying at 55 °C under vacuum over night, the electrodes were incorporated into 2016 coin-type cells in a glove box filled with Ar gas using lithium metal as the counter electrode, Cellgard 2400 microporous membrane as separator and 50 μL of 1 M bis-(trifluoromethane) sulfonimide lithium (LiTFSI, Alfa Corp.) in a mixture solution of dimethoxyethane (DME) and 1,3-dioxolane (DOL) (1:1,vol.%) as the electrolyte, The charge–discharge tests were carried out using a LAND Cell Test System (2001A, Wuhan, China) between cutoff voltage of 3 V and 1.5 V. Cyclic voltammetry (CV) tests in two electrode coin-type cells were performed between 1.5 V and 3 V at 0.1 mVs^{-1} on a CHI760D electrochemical work station.

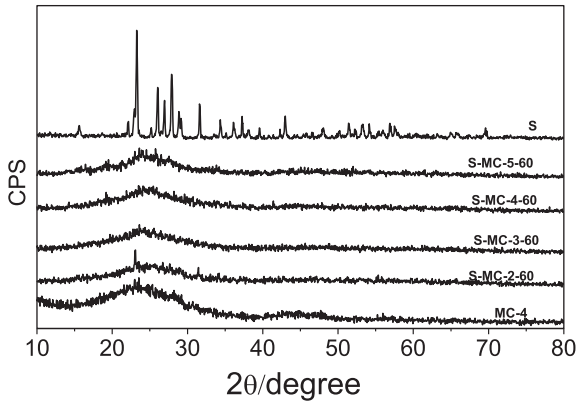

Fig. 1. XRD patterns of pristine sulfur, MC-4 spheres and four different S-MC-X-60 (X = 2, 3, 4 and 5, respectively) composite spheres with 60 wt% sulfur loading content.

3. Results and discussion

3.1. XRD

XRD patterns of the pristine sulfur powder, MC-4 spheres and a series of S-MC-X composite spheres with sulfur loading of 60 wt% are illustrated in Fig. 1. Sharp diffraction peaks of pristine sulfur indicated that the elemental sulfur exists in a crystalline state. The broad diffraction peaks around 24° and a weak peaks at 44° are observed in the pattern for MC-4 spheres, indicating an amorphous state [28–32]. However, the typical diffraction peaks of the crystalline sulfur disappeared entirely in all these S-MC-X-60 composite spheres, which can be ascribed to the incorporation of the sulfur into the interior of the mesopore and the homogeneous dispersion in them.

3.2. Raman spectra

Raman spectroscopy was extensively employed to characterize the structure of the amorphous MC spheres since the ratio of D-band to G-band (I_D/I_G) is sensitive to the disorder density of carbon materials. As can be seen from Fig. 2, the Raman spectrum of MC-4

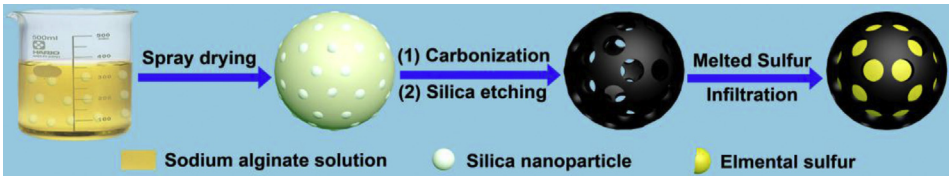

Scheme 1. Illustration for the formation process of the S-MC composite spheres.

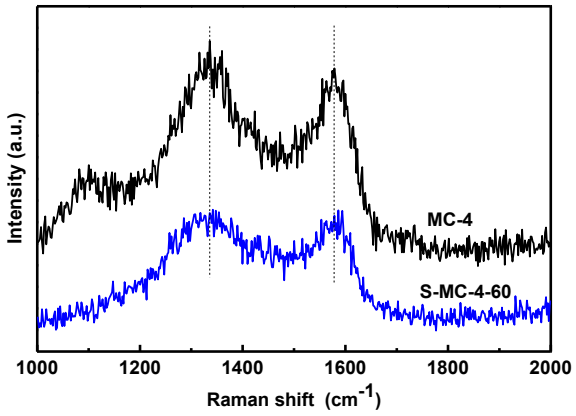

Fig. 2. Raman spectra of MC-4 spheres and S-MC-4-60 composite spheres.

spheres exhibits a D-band at 1335 cm^{-1} and a G-band at 1578 cm^{-1}, respectively, and the I_D/I_G ratio is 1.08. After the impregnation of sulfur with 60 wt% content, the center of the D-band and the G-band shifted to 1341 and 1586 cm^{-1}, respectively, while the intensity ratio of I_D/I_G for S-MC-4-60 composite spheres was decreased to 1, implying that the carbon matrix in S-MC-4-60 composite spheres turned to be more disordered after the incorporation of sulfur into the mesopores of the MC matrices.

3.3. Nitrogen adsorption-desorption measurements

Fig. 3 shows the nitrogen adsorption-desorption isotherms and corresponding pore size distribution curves of MC-X (X = 2, 3, 4 and 5) spheres and those of S-MC-X-60 composite spheres. As can be seen from Fig. 3 (a), all isotherms of these MC-X (X = 2, 3, 4 and 5) spheres show hysteresis loops and obvious capillary condensation steps, suggesting the existence of mesosized pores in them [33,34]. The corresponding pore size distribution curves demonstrated that the MC-X spheres possess abundant mesosized pores ranging from 12 to 30 nm (see Fig. 3(b)). Interestingly, additional pores with smaller sizes center around 9 nm appeared in MC-4 and MC-5 spheres. After the impregnation of sulfur, the resulting S-MC-X-60 showed also regular hysteresis loops and relative steep capillary condensation steps. However, in comparison with that of the pristine MC-X samples, the quantity of adsorbed nitrogen decreased drastically in the S-MC-X spheres due to the incorporation of sulfur into the pores, indicating further the reduction of the specific surface area and pore volume.

The values of the BET surface area, the total pore volume and the average pore diameter of the MC-X and the corresponding S-MC-X-60 samples were summarized in Table 1. From the table one can see that the BET surface area and the total pore volume of the S-MC-X composite spheres decreased drastically after the impregnation of sulfur in comparison with the corresponding MC-X, while the average pore diameter increased slightly and the small sized pores around 9 nm disappeared. For example, the MC-4 exhibits a relative high specific surface area of 1270 m^2g^{-1} and a large pore volume of 4.1 cm^3g^{-1}. After the loading of sulfur with 60 wt% content of the total mass, the specific surface area and total pore volume then decreased to 189 m^2g^{-1} and 0.78 cm^3g^{-1}, respectively. The reduction of the pore volume and specific surface area, especially the former case suggested that sulfur was mainly loaded inside the pores of the MC-X matrix since the sulfur particles anchored onto the external surface of the MC-X spheres would influence mainly on the specific surface area by modifying the area to mass ratio of the composite spheres, whereas the pore volume cannot be affected so dramatically by the externally anchored nanoparticles. While the slightly increase of the average pore size can be attributed to the strong capillary force in the small sized pores, which can adsorb the molten sulfur in advance than the large sized ones. As a result, only a part of the large sized pores were unoccupied finally as presented in Fig. 3 (c). Besides the specific surface area and pore volume, the information on the volume ratio of sulfur/carbon in the composite spheres may provide insight into the electrochemical performance of the sulfur–carbon composite materials. In theory, the volume of sulfur in the composite spheres can be deduced by subtracting the pore volume of the composite sphere from that of their counterparts, i.e. the corresponding pristine porous carbon microsphere. However, it is difficult to get the volume of the carbon substrates by such a strategy. Nevertheless, the carbon volume can be regarding as constant since all the S-MC-X-60 composite spheres are composed of 40 wt% of carbon and 60 wt% of sulfur, in which the carbon substrates originated from the same procedure. Then the variation of the volume ratio of sulfur/carbon in the S-MC-X-60 (X = 2, 3, 4 and 5) composite microspheres can be evaluated by estimating only the volume variation of sulfur. The volumes of sulfur in the S-MC-X-60 microspheres deduced by the pore volume subtracting method based on 1 unit of the composite samples are of 0.87, 1.36, 1.68 and 1.85 cm^3, respectively, for S-MC-2-60, S-MC-3-60, S-MC-4-60 and S-MC-5-60. It is obvious that the sulfur volume in the S-MC-X-60 composite microspheres increased with the increase of pore volume of the MC-X substrates. Whereas, the volume for 0.6 g of pristine crystalline sulfur is only 0.31 cm^3 calculated based on the sulfur density of 1.96 g/cm^3. The volumes of sulfur deduced with the pore volume subtracting method are much higher than that of the pristine sulfur with the same mass. The difference between them can be speculated as due to the density variation of sulfur in the MC-X substrates with different pore volumes. The high density of sulfur observed in the MC-2 substrate with a low pore volume may be ascribed to the space limiting effect during the deposition of sulfur into the pores of the carbon spheres. In contrast, the low-density sulfur obtained in the MC-4 microsphere with a large pore volume might be due to the large free volume for the sulfur deposition. The residual pore volume and specific surface area combined with the density of sulfur may play role coordinately in determining the electrochemical properties of the composite microspheres. For example, the low-density sulfur inside the pores of the MC-X substrates will be favorable to the diffusion of the electrolyte and the transportation of lithium ions. Detailed study on this issue is still underway in our group.

3.4. SEM and TEM measurements

Fig. 4 depicts the SEM images of a series of as-spraying-dried silica/SA composite microspheres consisting of SA and silica particles with different ratios. It can be seen that the SA/silica composite microspheres derived from suspension of different SA to silica ratios by spray-drying showed similar spherical morphology with a wrinkled surface and a size of 1–5 μm in diameter. From the images we can also see that the composite microspheres transformed into more irregular shapes and showed more obvious wrinkle structure with the increase of the content of silica colloid from 2 to 5 ml.

Pictures A to D of Fig. 5 display the SEM images of MC-X (X = 2, 3, 4 and 5) series samples derived from the corresponding SA/silica composite microspheres by carbonization and template etching processes. It can be seen that MC-2, MC-3 and MC-4 samples kept similar morphologies as the corresponding SA/silica composite microspheres. They showed also spherical morphology with a wrinkled surface and size diameters in the range of 1–5 μm. When the volume of the silica colloid increased to 5 mL, the small sized MC-5 shrank more obviously and showed more obvious wrinkle

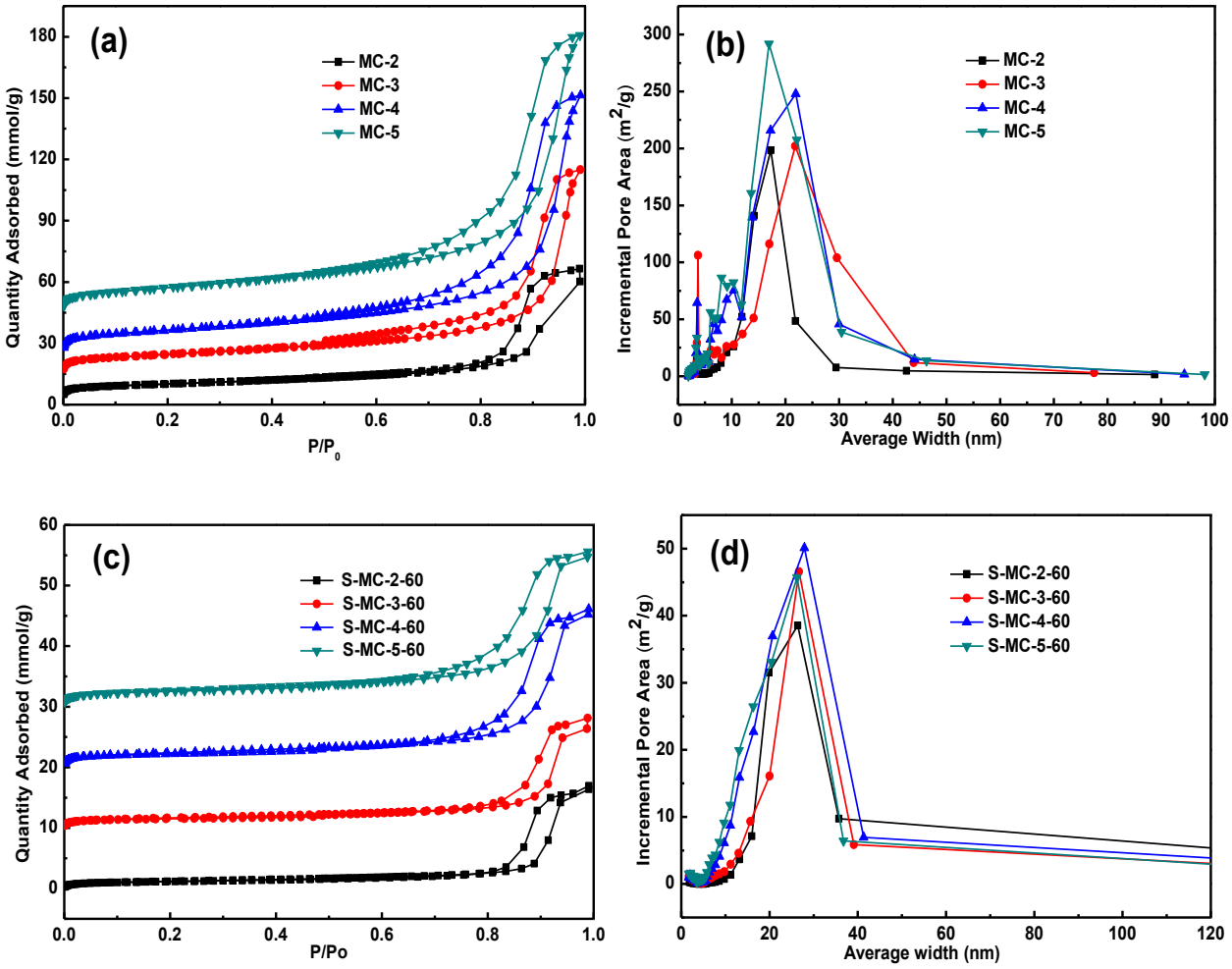

Fig. 3. Nitrogen adsorption–desorption isotherms (a, c) measured at 77 K and the corresponding pore size distribution (b, d) for the four different MC-X spheres before and after sulfur loading.

structure, while the large sized ones were broken into discrete fragments. From the broken fragments we can also deduce that some MC-5 spheres are hollow at the initial stage, and unfortunately the thin wall hollow carbon spheres did not keep the hollow structure during the carbonization step. Picture E of Fig. 5 depicts the TEM image of MC-4, which revealed clearly porous structure of the carbon sphere and supported the results of nitrogen sorption measurement. A zoom-in image in the picture for the region marked by the white rectangle shows that the MC-4 spheres are composed of abundant mesopores with the size around 20 nm, which will be in favor of the loading of elemental sulfur during the sulfur impregnation step and will also benefit for the infiltration of electrolyte and the fast transport of Li ions during the charge–discharge process. After the sulfur impregnation, the S-MC-4-60 composite spheres still could keep the original morphology of pristine MC-4 spheres, and no aggregated sulfur particles were observed on the external surface of the S-MC-4-60 composite spheres (see pictures C and F). The dispersion of carbon and sulfur in the composite spheres was characterized by the elemental map technique. The insets C (the red one) and S (the green one) in Fig. 5 F showed the elemental maps of carbon and sulfur elements, respectively, in a typical S-MC-4-60 composite sphere. The high contrast of the carbon map suggests that the surface of the composite spheres is composed mainly of carbon. On the other hand, it indicated that sulfur exists as small nanoparticles and is homogeneously dispersed in the mesopores of the MC-4 spheres.

Table 1
BET specific surface area and pore volume of MC-X spheres and the corresponding S-MC-X-W composite spheres.

Sample	BET surface area ($m^2 \cdot g^{-1}$)	Pore volume ($m^3 \cdot g^{-1}$)
MC-2	773	2.05
MC-3	1121	3.25
MC-4	1270	4.1
MC-5	1348	4.5
S-MC-2-60	95	0.36
S-MC-3-60	130	0.59
S-MC-4-60	189	0.78
S-MC-5-60	212	0.85

3.5. Electrochemical studies

Fig. 6(a) shows the cyclic voltammogram (CV) curves of the S-MC-4-60 composite material. In the first cathodic scan, two remarkable reduction peaks at 2.1 and 2.3 V, respectively, were detected. The upper plateau at 2.3 V corresponds to the reduction of elemental sulfur (S_8) or highly oxidized polysulfides such as Li_2S_8 and Li_2S_6 to Li_2S_4 [35–37], while the lower plateau at 2.1 V represents the reduction of Li_2S_4 or lower sulfides to Li_2S_2 or Li_2S. In the anodic scan, only one sharp oxidation peak is observed at the

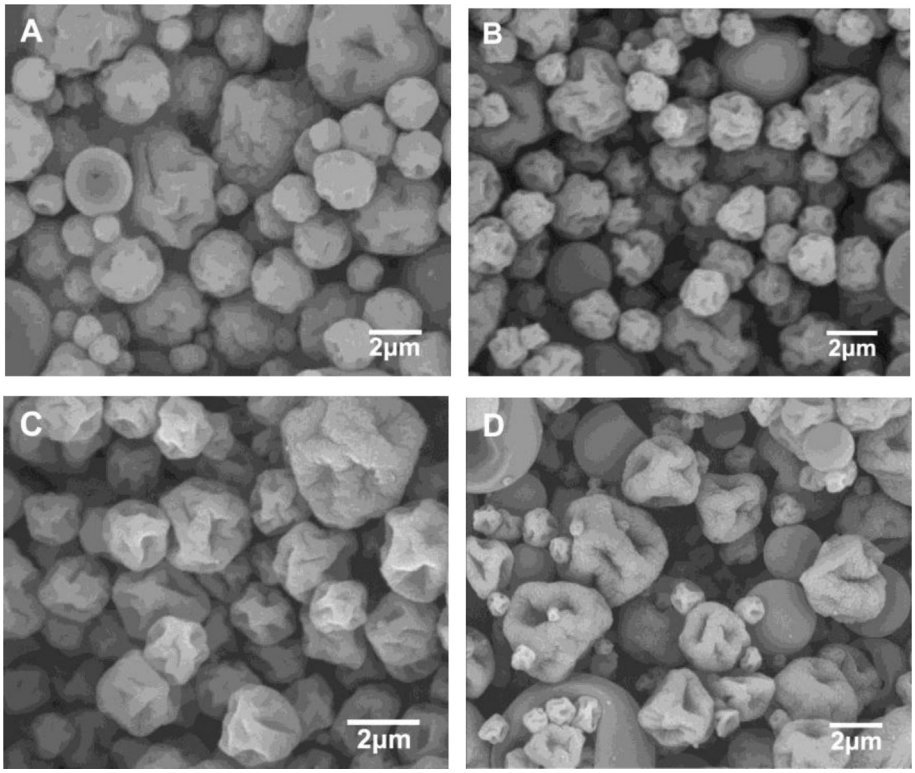

Fig. 4. SEM images of SA/silica composite microspheres derived from SA/silica suspensions with different silica colloid contents, (A) 2 mL, (B) 3 mL, (C) 4 mL, and (D) 5 mL.

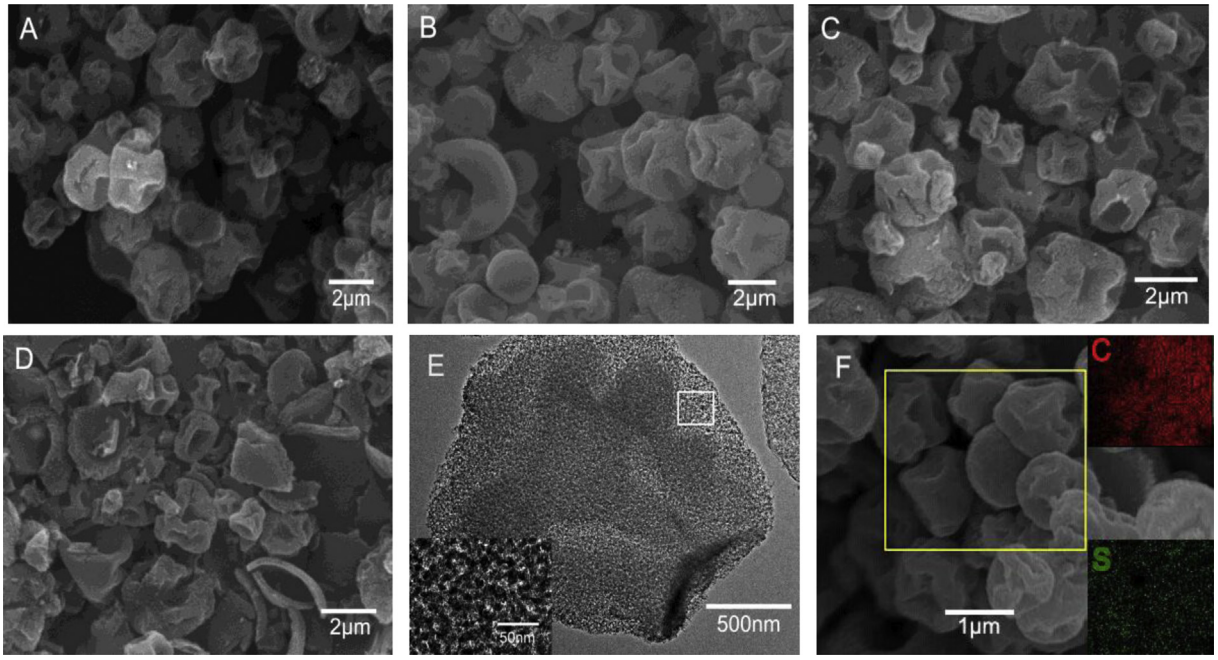

Fig. 5. SEM images of MC-2 (A), MC-3 (B), MC-4 (C) and MC-5 (D) samples, TEM image of MC-4 (E) (the inset in Figure E corresponds to the magnification of the white square area) and SEM image of S-MC-4-60 (F) (the red and the green insets in picture F showed the elemental maps of carbon and sulfur, respectively). (For interpretation of the references to color in this figure legend, the reader is referred to the web version of this article.)

potential of 2.45 V, which corresponds to the oxidation process of Li_2S [38,39]. The cathodic and anodic peak current densities of the sulfur–carbon composite spheres showed no obvious change after 5 cycling, illustrating that the cathode materials own excellent electrochemical reversibility due to the high porous structure and good electronic conductivity of the porous carbon matrices. The initial discharge–charge voltage profiles of the S-MC-2-60, S-MC-3-60 , S-MC-4-60 and S-MC-5-60 composite cathode materials at a 0.2C rate are depicted in panel (b) of Fig. 6. In the DME/DOL-based electrolyte, Li–S battery theoretically possesses two typical

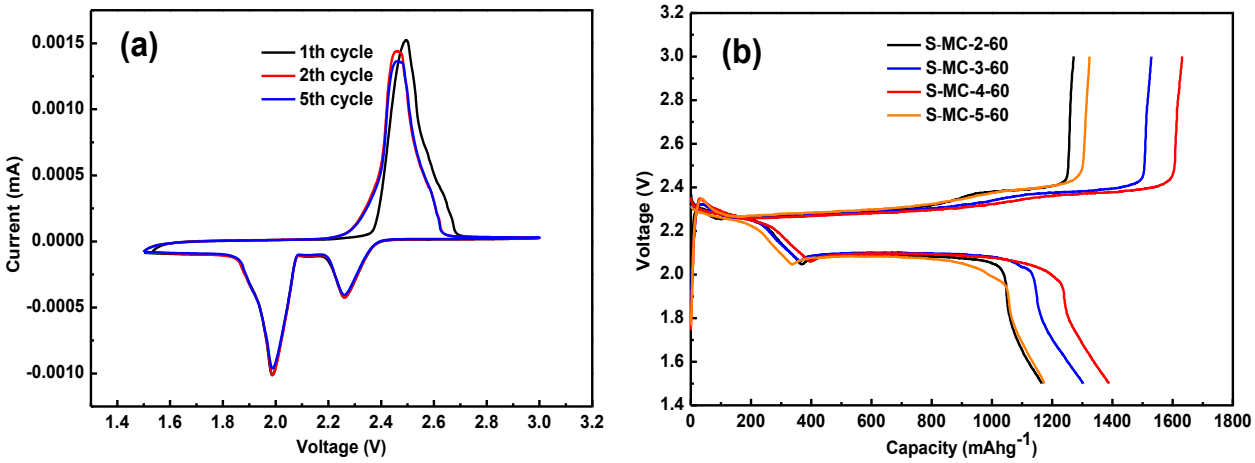

Fig. 6. (a) CV curve of S-MC-4-60 cathode measured under the potential window of 1.5–3.0 V at a scan rate of 0.1 mVs^{-1}, and (b) the initial discharge–charge voltage profiles of the four different composite cathodes at a rate of 0.2C.

discharge potential plateaus, which have been observed for all these cathodes, in accordance with the CV curves. The charge curves were also characterized by two plateaus at about 2.3 and 2.4 V. For the S-MC-4-60 composite cathode, although a small degree of overcharge exists, the initial discharge capacity can be as high as 1388 $mAhg^{-1}$, which reaches nearly up to 90% of the theoretical specific capacity of sulfur. The polysulfide shuttle phenomenon is still observed due to the soluble polysulfide diffusion from the external surface or the shallow channels close to the external surface of S-MC-X-60 composite spheres into the bulk electrolyte, which results in an overcharge to some extent. In contrast, S-MC-2-60 and S-MC-3-60 composite cathodes delivered initial discharge capacities of 1165 and 1252 $mAhg^{-1}$, respectively. Such decreases of the initial discharge capacities can be ascribed to the poor utilization of sulfur in the latter two matrices since their lower pore volume and specific surface area reduce the uptake of sulfur and the transportation of lithium ions. Whereas, S-MC-5-60 possessed high specific surface area and large pore volume but it showed the lowest specific discharge capacities. This might caused by the nonintegrated structure of the MC-5 spheres. More detailed discussion about this issue will be addressed in the following section.

Fig. 7 (a) depicts the discharge capacities of the different four S-MC-X-60 composite cathodes at various current rates. The discharge capacities decreased gradually as the rate increased from 0.2 to 2C for all of the four composite electrodes. It can be found S-MC-4-60 is superior to other S-MC-X-60 (X = 2, 3 and 5) composite cathodes in both the discharge capacity and the cycling stability. After a rapid decay from 1388 $mAhg^{-1}$ in the first cycle to 1253 $mAhg^{-1}$ in the second one at a current rate of 0.2C, the discharge capacity then faded gradually and was stabilized at around 1100 $mAhg^{-1}$. From the 21st cycle on, the current rates were increased firstly to 0.5C and then to 1 and 2C after each ten-cycle. It can be seen that the reversible capacity decreased slowly with the increase of the current rate. In addition, the S-MC-4-60 composite cathode could operate at a current rate as high as 2C and it still delivered a capacity of 864 $mAhg^{-1}$. When the rate was reset back to 0.2C regime after more than 50 cycles, the electrode resumed the original capacity of 1023 $mAhg^{-1}$ without abrupt capacity fading. However, for the other three composite cathodes, decreased reversible capacity and more rapid attenuation of capacity with the increase in current density can be clearly observed. Fig. 7 (b) shows the cycle performance of these four S-MC-X-60 (X = 2, 3,4 and 5) composite cathodes at a 0.2C rate in terms of up to 100 repeated discharge–charge galvanostatic cycles. It demonstrated that the S-MC-4-60 composite cathode delivered the best electrochemical

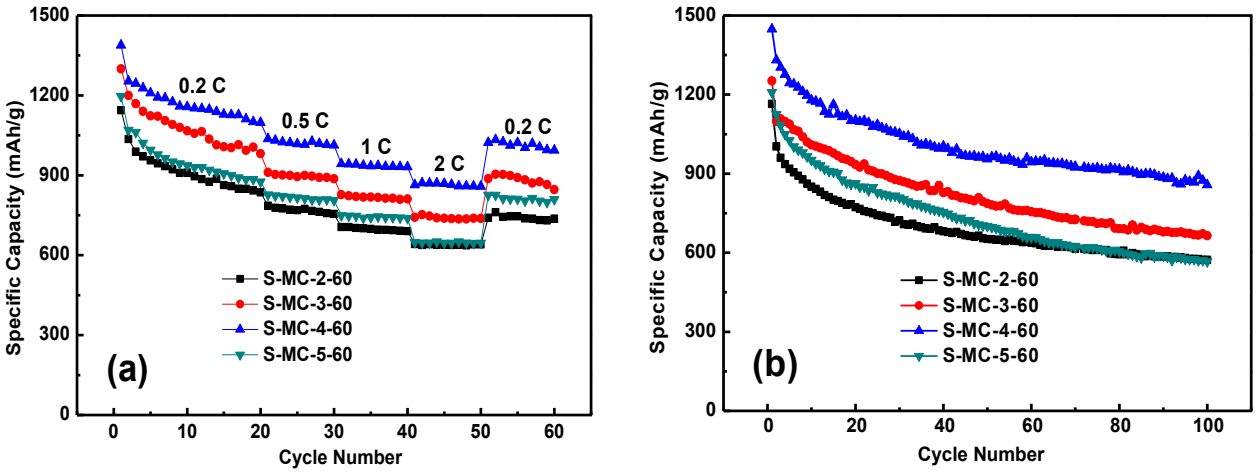

Fig. 7. (a) Multi-rate capabilities of the four different S-MC-X-60 composite spheres and (b) their cycling performance at 0.2C rate.

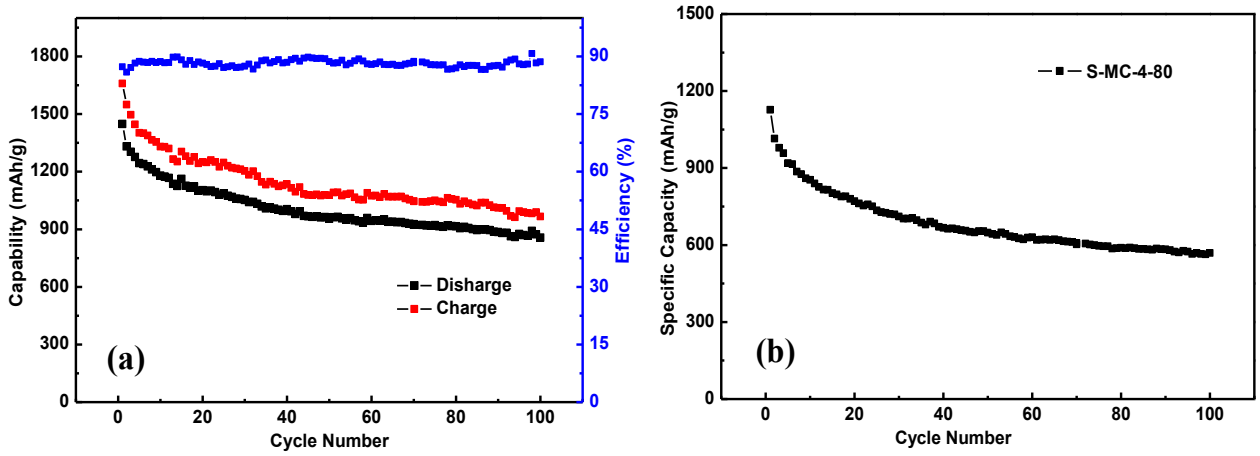

Fig. 8. (a) Cycling performance and coulombic efficiency of S-MC-4-60 composite spheres and (b) Cycling performance of S-MC-4-80 composite spheres.

performance with enhanced capacity retention, and it could retain an outstanding capacity as high as 857 $mAhg^{-1}$ after 100 cycles. The relatively high rate capability for S-MC-4-60 electrode may be attributed to the good electrical conductivity originating from the integrated spherical structure and to the high transportation rates of lithium ions and solvated electrolyte derived from the high pore volume and the relative large specific surface area.

From the above discussion we can deduce that S-MC-4-60 cathode showed more promising electrochemical performance than the other three composite cathodes of S-MC-2-60, S-MC-3-60 and S-MC-5-60. The differences of the electrochemical performance among the four cathodes can be ascribed to the difference of the structure perfection, specific surface area, and total pore volume and pore size distribution. In the case of S-MC-4-60 cathode, the relative high specific surface area originated from the meso-sized channels provides the large interfacial contact area between sulfur and carbon at the nanoscale and the boundless interconnects of the MC-4 framework for electron conduction. The relatively high specific surface area could also introduce electrolyte into the active cathode material to maintain the intimate contact with conductive carbon matrix and supply more electrochemical reaction sites. As a result, the negative effects of dissolution of polysulfide and the insulation of sulfur could be minimized.

The large pore volume and hierarchical pore structures could provide commendable pore volume to accommodate the volumetric expansion of sulfur upon uptake of lithium ions and restrict the diffusion of the polysulfides during the charge/discharge process. As can be seen from the nitrogen sorption measurements that the small sized pores were filled firstly due to the strong capillary force in them and some large sized pores were unoccupied. The residual pore volume from 'unstuffed' large sized mesopores can not only facilitate the transport of lithium ions inside the carbon spheres but also accommodate the soluble polysulfide during the reaction. As for the S-MC-2-60 and S-MC-3-60 composite spheres, low specific surface area limited the complete interfacial contact between sulfur and carbon at a nanoscale, while the reduced pore volume may result in crowding in the mesopore of the MC-X spheres by excess sulfur, which retarded both the electron and ion transports and lowered the ability to uptake lithium ions, bringing down the utilization of active sulfur. This phenomenon was widely observed in the S-MC-X composites with a high sulfur loading. In addition, the integrity of morphology and perfection of structure for MC-X is also an important factor for sulfur accommodation and electron transportation when they were used as matrices for Li–S battery. For example, S-MC-5-60 composite spheres possess the largest pore volume and the highest specific surface area among the four kinds of composite spheres, but it delivered quite similar electrochemical performance to S-MC-2-60 only. Such a result might be ascribed to the broken structure of MC-5 spheres, which impaired its capacity of accommodating lithium polysulfides and resulted in its direct dissolution into electrolyte from the shallow opening of the channel closed to the external surface, leading to the loss of active material. All in all, S-MC-4 can be considered as the most optimistic material among them due to its unique mesoporous structure, relative large pore volume, high specific surface area and integrated spherical structure, all of which are crucial for achieving both high sulfur loading and good electrochemical performance.

The sulfur shuttle effect is a typical phenomenon in Li–S batteries, which usually results in imperfect charging and decrease of discharge capacity and leads to a low coulombic efficiency of the cell. The charge/discharge capacity of S-MC-4-60 composite cathode at a current rate of 0.2C and the corresponding coulombic efficiency are shown in Fig. 8 (a). Considering the high sulfur loading content in S-MC-4-60 composite spheres and no further process to evaporate the residual sulfur on the external surface of S-MC-X, the soluble polysulfide located at the external surface or the shallow channels of the S-MC-X spheres could diffuse into the bulk electrolyte during the charge/discharge process, resulting in the overcharge phenomena and reducing the coulombic efficiency. On the basis of the above discussion, one can deduced that the MC-4 spheres are the optimistic matrix for the preparation of cathode for Li–S battery with 60 wt% sulfur content. In order to improve the energy density of the composite cathode and further investigate the limitation of MC-X as conductive matrices, MC-4 spheres were utilized as support for the preparation of composite cathode materials with 80 wt% sulfur content and the cycle performance of the S-MC-4-80 is presented in Fig. 8 (b). It can be seen that the S-MC-4-80 composite cathode could deliver an initial capacity of 1127 $mAhg^{-1}$ at 0.2C and the capacity remained at 569 $mAhg^{-1}$ after 100 cycles, which showed still very excellent performance and potential to industrial application.

4. Conclusions

In summary, a promising approach to the total-preparation of sulfur-impregnated mesoporous carbon (S-MC) composite spheres as cathode materials for Li–S battery has been demonstrated. As good conductive matrix and inclusion substrate for sulfur, the mesoporous carbon spheres with hierarchical pores, controlled

pore volume and specific surface areas were successfully prepared through a mass-producible spray drying assisted template method using sodium alginate as carbon precursor and commercial silica nanoparticles as pore directing templates. Four kinds of MC spheres with controlled specific surface area from 773 to 1348 m^2g^{-1} and pore volume from 2.0 to 4.5 cm^3g^{-1} were obtained by tuning the ratio between the carbon precursor and the pore directing agent. The four kinds of pristine MC spheres could be used as conductive substrates for preparing cathode of rechargeable Li–S batteries, which demonstrated different electrochemical performance due to the porosity and structure variation among them. The autogenetic high-pressure induced impregnation is efficient for loading sulfur into the pores of the MC spheres and no extra step for the evaporation of the externally anchored sulfur was required. With this method, sulfur-impregnated MC composite spheres with sulfur loading content up to 80 wt% of the total mass can then be obtained. For the S-MC-4-60 composite cathode materials, a discharge capacity of 864 $mAhg^{-1}$ was achieved at 2C current density and the capacity was maintained at 857 $mAhg^{-1}$ after 100 cycles at 0.2C. Even for S-MC-4-80, it could still remain 569 $mAhg^{-1}$ after 100 cycles at 0.2C. The high specific surface area, large internal pore volume and integrated structure of the MC spheres could be the crucial factors in determining their electrochemical performance as cathode for Li–S battery. The electronically conductive MC matrices provide abundant surface area and high pore volume to disperse and adopt sulfur. As a result, the disadvantages of sulfur used as cathode materials for Li–S battery then can be ameliorated rationally by repressing the volume expansion of sulfur and reducing the shuttling loss of polysulfides. Therefore, the cycle stability and the utilization of sulfur for the Li–S batteries have been significantly improved. In a word, the MC with hierarchical pores, controlled pore volume, high specific surface areas and perfect structures can compromise both high sulfur loading and excellent electrochemical performance. It is believed that the MC with mesoporous structures and controlled pore volume can also be generalized to other practical applications.

Acknowledgments

This work is supported by the National Key Project on Basic Research (Grant No. 2012CB722705), the National High Technology Research and Development Program of China (Nos. 2012AA110407 and 2014AA052303) and the Natural Science Foundation of China (Nos. 21103096 and U1232104). Y. Q. Wang would like to thank the financial support from the Top-notch Innovative Talent Program of Qingdao City (Grant no.: 13-CX-8) and the Taishan Scholar Program of Shandong Province.

References

[1] T.D. Bogart, D. Oka, X.T. Lu, B.A. Korgel, ACS Nano 8 (2014) 915–922.
[2] E.M. Erickson, C. Ghanty, D. Aurbach, J. Phys. Chem. Lett. 5 (2014) 3313–3324.
[3] H.S. Li, L.F. Shen, K.B. Yin, J. Ji, J. Wang, X.Y. Wang, X.G. Zhang, J. Mater. Chem. A 1 (2014) 7270–7276.
[4] J.H. Yang, J. Tan, D. Ma, J. Power Sources 260 (2014) 169–173.
[5] Y.X. Yin, S. Xin, Y.G. Guo, L.J. Wan, Angew. Chem. Int. 52 (2013) 13186–13200.
[6] G.Y. Xu, B. Ding, J. Pan, P. Nie, L.F. Lai, X.G. Zhang, J. Mater. Chem. A 2 (2014) 12662–12676.
[7] Q. Li, Z.A. Zhang, K. Zhang, J. Fang, J. Li, J. Power Sources 256 (2014) 137–144.
[8] L. Chen, L.L. Shaw, J. Power Sources 267 (2014) 770–783.
[9] F. Wu, J. Chen, R. Chen, S. Wu, L. Li, S. Chen, T. Zhao, J. Phys. Chem. C 115 (2011) 6057–6063.
[10] Y. Fu, A. Manthiram, RSC Adv. 2 (2012) 5927–5929.
[11] Y.S. Su, Y. Fu, A. Manthiram, Phys. Chem. Chem. Phys. 14 (2012) 14495–14499.
[12] H. Ye, Y.-X. Yin, S. Xin, Y.-G. Guo, J. Mater. Chem. A 1 (2013) 6602–6608.
[13] L. Qie, W. Chen, H. Xu, X. Xiong, Y. Jiang, F. Zou, X. Hu, Y. Xin, Z. Zhang, Y. Huang, Energy Environ. Sci. 6 (2013) 2497–2504.
[14] H. Wang, Y. Yang, Y. Liang, J.T. Robinson, Y. Li, A. Jackson, Y. Cui, H. Dai, Nano Lett. 11 (2011) 2644–2647.
[15] X.Z. Ma, B. Jin, P.M. Xin, H.H. Wang, Appl. Surf. Sci. 307 (2014) 346–350.
[16] D. Li, F. Han, S. Wang, F. Cheng, W.C. Li, ACS Appl. Mater. Interface 5 (2013) 2208–2213.
[17] L. Yu, N. Brun, K. Sakaushi, J. Eckert, M.M. Titirici, Carbon 61 (2013) 245–253.
[18] Q. Li, Z. Zhang, Z. Guo, Y. Lai, K. Zhang, J. Li, Carbon 78 (2014) 1–9.
[19] X. Tao, X. Chen, Y. Xia, H. Huang, Y. Gan, R. Wu, F. Chen, W. zhang, J. Mater. Chem. A 1 (2013) 3295–3301.
[20] C. Zhao, L. Liu, H. Zhao, A. Krall, Z. Wen, J. Chen, P. Hurley, J. Jiang, Y. Li, Nanoscale 6 (2014) 882–888.
[21] M. He, L.X. Yuan, W.X. Zhang, X.L. Hu, Y.H. Huang, J. Phys. Chem. C 115 (2011) 15703–15709.
[22] S. Evers, T. Yim, L.F. Nazar, J. Phys. Chem. C 116 (2012) 19653–19658.
[23] J.W. Choi, G. Cheruvally, D.S. Kim, J.H. Ahn, K.W. Kim, H.J. Ahn, J. Power Sources 183 (2008) 441–445.
[24] C. Liang, Z. Li, S. Dai, Angew. Chem. Int. 47 (2008) 3696–3717.
[25] B. Zhang, X. Qin, G.R. Li, X.P. Gao, Energy Environ. Sci. 3 (2010) 1531–1537.
[26] K. Xi, S. Cao, X. Peng, C. Ducati, R. Vasant Kumar, A.K. Cheetham, Chem. Commun. 49 (2013) 2192–2194.
[27] C. Zu, A. Manthiram, Adv. Energy Mater. 3 (2013) 1008–1012.
[28] M.S. Park, J.S. Yu, K.J. Kim, G. Jeong, J.H. Kim, Y.N. Jo, U. Hwang, S. Kang, T. Woo, Y.-J. Kim, Phys. Chem. Chem. Phys. 14 (2012) 6796–6804.
[29] J. Zhang, Z.M. Dong, Q.M. Su, G.H. Du, J. Power Sources 270 (2014) 1–8.
[30] C.M. Xu, Y.S. Wu, G.H. Du, J.P. Tu, J. Power Sources 275 (2015) 22–25.
[31] B. Ding, C.Z. Yuan, L.F. Shen, G.Y. Xu, P. Nie, X.G. Zhang, J. Mater. Chem. A 1 (2013) 1096–1101.
[32] C.F. Zhang, H.B. Wu, C.Z. Yuan, Z.P. Guo, Angew. Chem. Int. 51 (2012) 9592–9595.
[33] X. Liang, M. Kaiser, K. Konstantinov, R. Tandiono, H.K. Liu, S.X. Dou, J.Z. Wang, J. Mater. Chem. A 4 (2014) 36513–36516.
[34] Q. Li, Z. Zhang, K. Zhang, J. Li, Carbon 78 (2014) 1–9.
[35] Y. Jung, S. Kim, Electrochem. Commun. 9 (2007) 249–254.
[36] J. Zhang, H. Ye, Y. Yin, Y. Guo, J. Energy Chem. 23 (2014) 308–314.
[37] J.R. Akridge, Y.V. Mikhaylik, N. White, Solid State Ionics 175 (2004) 243–245.
[38] X. Liang, Z.Y. Wen, L.Z. Huang, J. Jin, J. Power Sources 196 (2011) 3655–3658.
[39] G.Q. Ma, Z.Y. Wen, J. Jin, J.C. Zhang, J. Power Sources 254 (2014) 353–359.